Am J Physiol Heart Circ Physiol 295: H1141–H1149, 2008.
First published July 11, 2008; doi:10.1152/ajpheart.00284.2008.

Material properties of the ovine mitral valve anterior leaflet in vivo from inverse finite element analysis

Gaurav Krishnamurthy,[1,2] Daniel B. Ennis,[1] Akinobu Itoh,[1] Wolfgang Bothe,[1] Julia C. Swanson,[1] Matts Karlsson,[3] Ellen Kuhl,[2] D. Craig Miller,[1] and Neil B. Ingels Jr.[1,4]

Departments of [1]Cardiothoracic Surgery and [2]Mechanical Engineering, Stanford University, Stanford, California; [3]Department of Management and Engineering, Linköping University, Linköping, Sweden; and [4]Laboratory of Cardiovascular Physiology and Biophysics, Research Institute of the Palo Alto Medical Foundation, Palo Alto, California

Submitted 15 March 2008; accepted in final form 8 July 2008

Krishnamurthy G, Ennis DB, Itoh A, Bothe W, Swanson JC, Karlsson M, Kuhl E, Miller DC, Ingels NB Jr. Material properties of the ovine mitral valve anterior leaflet in vivo from inverse finite element analysis. *Am J Physiol Heart Circ Physiol* 295: H1141–H1149, 2008. First published July 11, 2008; doi:10.1152/ajpheart.00284.2008.—We measured leaflet displacements and used inverse finite-element analysis to define, for the first time, the material properties of mitral valve (MV) leaflets in vivo. Sixteen miniature radiopaque markers were sewn to the MV annulus, 16 to the anterior MV leaflet, and 1 on each papillary muscle tip in 17 sheep. Four-dimensional coordinates were obtained from biplane videofluoroscopic marker images (60 frames/s) during three complete cardiac cycles. A finite-element model of the anterior MV leaflet was developed using marker coordinates at the end of isovolumic relaxation (IVR; when the pressure difference across the valve is ~0), as the minimum stress reference state. Leaflet displacements were simulated during IVR using measured left ventricular and atrial pressures. The leaflet shear modulus ($G_{circ\text{-}rad}$) and elastic moduli in both the commissure-commisure (E_{circ}) and radial (E_{rad}) directions were obtained using the method of feasible directions to minimize the difference between simulated and measured displacements. Group mean (±SD) values (17 animals, 3 heartbeats each, i.e., 51 cardiac cycles) were as follows: $G_{circ\text{-}rad} = 121 \pm 22$ N/mm^2, $E_{circ} = 43 \pm 18$ N/mm^2, and $E_{rad} = 11 \pm 3$ N/mm^2 ($E_{circ} > E_{rad}$, $P < 0.01$). These values, much greater than those previously reported from in vitro studies, may result from activated neurally controlled contractile tissue within the leaflet that is inactive in excised tissues. This could have important implications, not only to our understanding of mitral valve physiology in the beating heart but for providing additional information to aid the development of more durable tissue-engineered bioprosthetic valves.

mitral valve material properties; inverse finite-element analysis; ovine model; radiopaque markers

THE MITRAL VALVE (MV) cycles roughly 100,000 times/day, opening widely in <100 ms during each heart beat to allow the rapid diastolic inflow of blood into the left ventricle (LV) from the low-pressure left atrium (LA) and then closing tightly in <100 ms to prevent backflow into the LA during high-pressure LV ejection.

Although the valve performs this function normally in most hearts for as many as 3×10^9 cycles in a human lifetime, MV dysfunction afflicts millions worldwide, and more than 300,000 patients each year undergo open-heart surgery to treat malfunctioning or diseased heart valves. While surgical valve repair is preferred, valve replacement may be necessary. Replacement involves the implantation of a mechanical or tissue valve, which is associated with anticoagulation/thromboembolic complications and less than ideal durability, respectively. To overcome these limitations, a currently important research goal is to create bioengineered, autologous tissue valves. A more complete understanding of the material properties of native MV leaflets is important for this task.

Studies of porcine and human MVs ex vivo have demonstrated that the material properties of the anterior leaflet are consistent with the behavior of compliant collagen membranes, with pretransitional moduli of 0.02–0.09 N/mm^2 and posttransitional moduli of 0.2–9.0 N/mm^2 (8, 22, 33, 42). Supporting this concept of highly compliant leaflets is the common sight in the operating room that the anterior leaflet bulges toward the LA, uniformly concave to the LV cavity, during LV test inflations (3). Further support arises from a study of casts from inflated excised hearts displaying this same leaflet curvature (34). These findings have led to the traditional view that the anterior leaflet is curved uniformly concave to the LV cavity during systole in the beating heart, and computational models of the mitral valve to date have employed such curvature (35, 39, 41, 46, 47, 50, 51).

Our studies, however, have demonstrated that the anterior leaflet midline, rather than exhibiting uniform curvature concave to the LV, displays a compound curvature in the beating heart, convex to the LV in the half nearest the annulus and concave to the LV nearest the leaflet edge (30). This compound curvature poses an important fundamental challenge to our understanding of the MV. How can a thin (~1 mm thick) flexible leaflet with an elastic modulus of <10 N/mm^2 support maximum LV pressure (LVP) without bending concave to the LV? Clearly, the maintenance of this convex curvature requires some form of additional support.

The most obvious candidates for this support are the chordae tendineae attached to the leaflets. A network of primary (first order) chords runs from each papillary muscle tip to the leaflet free edges. But these primary chords cannot be the support needed because they attach only to the leaflet edges and thus could not prevent the flexible leaflet belly, suspended between the annulus and the free edge, from ballooning into the LA. This leaves the second-order (strut) chords as possibilities. Strut chords from each papillary muscle are positioned to help support the anterior leaflet belly on the associated side of the leaflet midline, but when we recently compared anterior leaflet

Address for reprint requests and other correspondence: N. B. Ingels, Jr., Laboratory of Cardiovascular Physiology and Biophysics, Research Institute, Palo Alto Medical Foundation, AMES Bldg., 795 El Camino Real, Palo Alto, CA 94301-2302 (e-mail: ingels@stanford.edu).

The costs of publication of this article were defrayed in part by the payment of page charges. The article must therefore be hereby marked "*advertisement*" in accordance with 18 U.S.C. Section 1734 solely to indicate this fact.

midline shape in beating hearts before and after cutting major branches of both strut chords, the compound leaflet curvature was virtually unchanged (48).

This suggested the possibility that the leaflets are able to resist high LV systolic pressure because they are much stiffer in vivo than in vitro. But why would the leaflets be so much stiffer in the beating heart than when isolated? The answer may be straightforward: the leaflets are not just passive collagen structures, their composition includes large quantities of excited, neurally controlled contractile tissue, and this tissue, inactive in studies of isolated tissues, may be active to stiffen the leaflets in the intact beating heart (59). Employing marker measurements and an inverse finite-element approach, we therefore tested the hypothesis that leaflets in the beating ovine heart in vivo were much stiffer than in vitro values obtained to date from isolated tissues.

METHODS

All animals received humane care in compliance with the "Principles of Laboratory Animal Care" formulated by the National Society for Medical Research and also in compliance with the National Institutes of Health *Guide for the Care and Use of Laboratory Animals* (NIH Pub. 85-23, Revised 1985). This study was approved by the Stanford Medical Center Laboratory Research Animal Preview Committee, which is accredited by the Association for Assessment and Accreditation of Laboratory Animal Care International, and was conducted according to Stanford University policy.

Surgical Preparation

Seventeen adult, Dorset-hybrid, male sheep (54 ± 8 kg) were premedicated with ketamine (25 mg/kg im) for venous and arterial catheter placement and checked for mitral regurgitation by transesophageal Doppler echocardiography. Animals without mitral regurgitation were anesthetized with inhalational isoflurane (1.0–2.5%), intubated, and mechanically ventilated. Through a left thoracotomy, 13 miniature radiopaque tantalum markers were surgically implanted into the subepicardium to silhouette the LV chamber along 4 equally spaced longitudinal meridians (ventricular markers, Fig. 1*A*). On cardiopulmonary bypass, a total of 35 radiopaque tantalum markers were sewn to the following sites: 1 marker at the tip of each papillary muscle [anterior (APM) and posterior papillary muscle (PPM), Fig. 1*A*], 16 markers around the mitral annulus (annular markers, Fig. 1*A*), 16 markers on the atrial aspect of the anterior MV leaflet [7 on the MV leaflet edge (*markers 1–7*, Fig. 1*B*) and 9 on the leaflet belly (*markers 8–16*, Fig. 1*B*)], and 1 marker on the central edge of the middle scallop of the posterior mitral leaflet (Fig. 1*A*). A single tantalum loop (0.6 mm inner diameter and 1.1 mm outer diameter, 3.2 mg each) was used for each leaflet marker (Fig. 2). Animals were weaned from cardiopulmonary bypass, and a micromanometer transducer (PA4.5-X6, Konigsberg Instruments, Pasadena, CA) was placed in the LV through the LA.

Data Acquisition

Animals were transferred to the experimental catheterization laboratory and placed in the right lateral decubitus position for the acquisition of data under open-chest conditions. Two micromanometer pressure transducers (model MPC-500, Millar Instruments, Houston, TX), water column calibrated to define scaling and offset factors, were introduced into the LV via the carotid artery. The Konigsberg catheter was advanced from the LA into the LV, and the Konigsberg and Millar transducer signals recorded simultaneously. Linear regression of the Konigsberg signal on the LV Millar signal was performed to define the factors (both slope and intercept) to apply to the Konigsberg signal to match the LV Millar pressure measurement. The Konigsberg transducer was then pulled back into the LA for LA pressure (LAP) measurements, and one of the Millar pressure transducers was pulled back into the aorta for aortic pressure (AoP) measurements immediately distal to the aortic valve.

Videofluoroscopic images (60 frames/s) of all radiopaque markers were acquired using a biplane videofluoroscopy system (Philips Medical Systems, Pleasanton, CA) with the heart in normal sinus rhythm and ventilation transiently arrested at end expiration. Marker coordinates from each view were then merged to yield three-dimensional coordinates of the centroid of each marker in each frame using semiautomated image processing and digitization software developed in this laboratory (43), accurate to 0.1 ± 0.3 mm (14). LVP, LAP, AoP, and electrocardiographic voltage signals were digitally recorded simultaneously during marker data acquisition and synchronized to the image acquisition. After data acquisition, animals were euthanized, and hearts were excised. Ex vivo photographs of the MV and subvalvular apparatus were used to generate insertion points for the chordae tendinae on the MV leaflet for the finite-element model.

Hemodynamics and Cardiac Cycle Timing

Three consecutive beats in sinus rhythm were selected for analysis from each heart. For each beat, end systole was defined as the frame containing the minimum second derivative of LVP with respect to time. $-dP/dt_{max}$ was computed as the maximum time derivative of LVP during isovolumic relaxation (IVR). The onset of isovolumic relaxation (IVR1; Fig. 3) was defined at end systole, and the end of IVR (IVR2; Fig. 3) was defined as the frame immediately before MV opening, as the earliest increase (above the systolic variation) in the separation between the central anterior and posterior leaflet edge markers (Fig. 3). The finite-element analysis was performed in the interval from IVR1 to IVR2, when the valve is closed, to *1*) allow the definition of transleaflet pressure that is otherwise indeterminate and *2*) eliminate flow-dependant issues, as LV volume does not change during this interval.

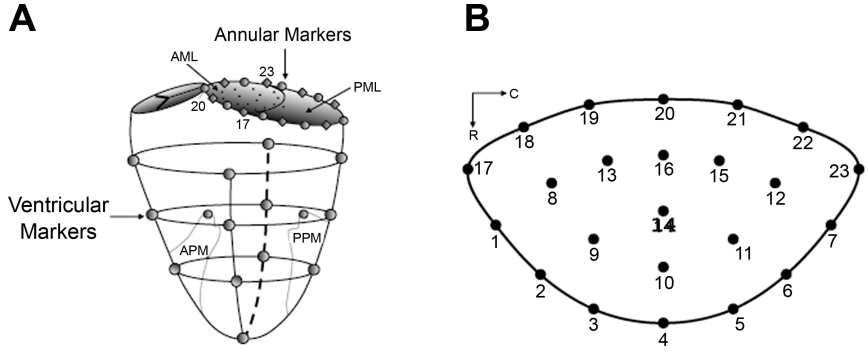

Fig. 1. *A*: schematic showing ventricular and annular marker locations. AML, anterior mitral leaflet; PML, posterior mitral leaflet; APM, anterior papillary muscle; PPM, posterior papillary muscle. *B*: schematic template showing the anterior leaflet marker grid as viewed from the left atrium (LA). *Marker 20* is the anterior leaflet saddlehorn marker; *marker 4* is the central meridian leaflet edge marker; and *markers 17* and *23* are the commissural markers. The group mean leaflet dimension from *marker 20* to *marker 4* was 1.9 ± 0.2 cm; the group mean leaflet marker dimension from *marker 17* to *marker 23* was 3.7±0.7 cm. *Inset*, radial (*R*) and circumferential (*C*) axes for material property definitions.

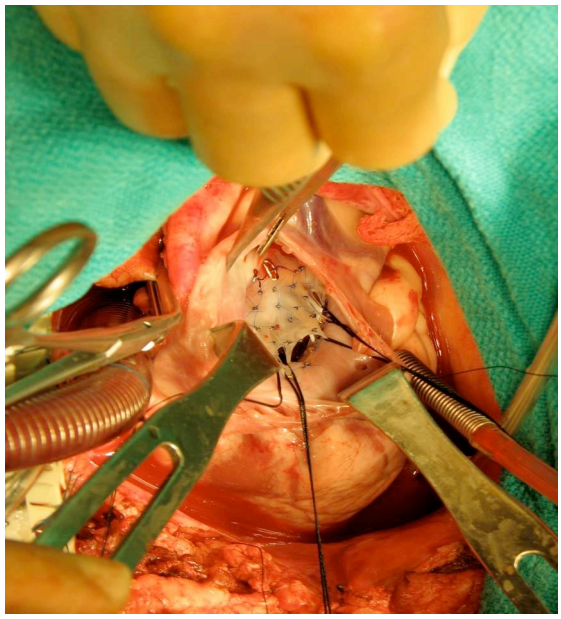

Fig. 2. Intraoperative photograph of the ovine mitral valve showing radiopaque markers sewn to the anterior leaflet and annulus.

Inverse Finite-Element Analysis

Finite-element model. A finite-element model of the anterior MV leaflet was developed using Hypermesh version 8.0 SR 1 (Altair Hyperworks, Troy, MI) to construct the geometry and meshing of the leaflet and Optistruct version 8.0 SR 1 (Altair Hyperworks) as the solver.

The geometry of the anterior leaflet was initially defined by the leaflet marker positions measured in Euclidian laboratory coordinates (Fig. 1) at IVR2 (assumed as the minimum stress reference state). These *x*,*y*,*z*-coordinate values for each of the leaflet and annular marker positions at IVR2 were entered as points in Hypermesh. Five cubic splines were generated through (see Fig. 1B) the following: *1*) *markers 17-1-2-3-4-5-6-7-23*, *2*) *markers 18-8-9-10-11-12-22*, *3*) *markers 19-13-14-15-21*, *4*) *markers 19-16-21*, and *5*) *markers 19-20-21*. These splines were used to generate a bicubic leaflet surface.

For the purpose of defining MV leaflet material properties, a polar coordinate system was then defined with origin at the center of the 16 markers defining the saddle-shaped annulus (38) at IVR2. A line from the origin to *marker 20* (the "saddlehorn") was defined as the leaflet radial axis (*R*, Fig. 1). The leaflet circumferential axis (*C*, Fig. 1) was defined normal to *R* and in the plane containing *R* and the posterior commissural marker (*marker 23*, Fig. 1). These commonly used axes sufficed for this initial effort to solve for the in vivo orthotropic material properties of the anterior MV leaflet belly and allowed comparison with previous studies. As more is known about leaflet microstructure (e.g., fiber and contractile tissue orientation, variation in architecture throughout the leaflet thickness, etc.), however, more sophisticated coordinate systems will likely need to be employed to more appropriately map the heterogeneous properties of the leaflet.

The material model of the leaflet was assumed to be orthotropic linear elastic (MAT8 material model in Hypermesh). Material property values [elastic modulus in the commisure-commisure direction (E_{circ}) = 6.23 N/mm^2, elastic modulus in the radial direction (E_{rad}) = 2.35 N/mm^2, leaflet shear modulus ($G_{circ\text{-}rad}$) = 1.369 N/mm^2, and leaflet density = 0.0011 kg/cm^3] obtained from excised porcine MV tissue (47) were used as initial material parameters to seed the material parameter identification algorithm.

Two separate shells (PSHELL in Hypermesh) were used to define the varying thickness of the leaflet regions using data obtained from our histological study of an anterior leaflet from a representative ovine heart. The first shell defined a region radiating from the annulus saddlehorn marker (*marker 20*) to 75% of the leaflet toward the free edge; this region had thickness values that varied linearly from 1.2 mm at the annulus to 0.7 mm 75% toward the leaflet free edge. The second shell defined the remaining 25% of the leaflet with a uniform thickness value of 0.2 mm. The measured thickness change from 0.2 to 0.7 mm at the 75% boundary reflects the presence of strut chords that insert at that boundary.

The bicubic surface fit of the MV leaflet was then meshed with two-dimensional noded plane-stress quadrilateral shell elements. An element size of 0.004 cm^2 was selected, yielding a mesh size of ~2,200 elements for a typical anterior leaflet. This mesh size yielded a total computational time of 1.5 min for each material parameter identification run, allowing experimental displacements to be matched with <5% error for the final material properties obtained.

The strut chordae were defined as structures undergoing pure tension (MAT1 in Hypermesh). A previously published ex vivo modulus [elastic modulus = 20 N/mm^2 and cross-sectional area = 0.008 cm^2 (33)] was used for the strut chordae. Tension-only bar elements (PBARL in Hypermesh) were defined as radiating from the papillary muscle tip marker points (APM and PPM, Fig. 1*A*) to leaflet belly insertion positions (Fig. 4) defined from the anatomic photographs (e.g., Fig. 2).

The boundary conditions were then enforced on the finite-element model. The change in measured LVP from IVR2 to IVR1 was applied to the ventricular surface of the anterior MV leaflet, and the change in measured LAP from IVR2 to IVR1 was applied to the atrial surface of the leaflet. The displacements of annular markers (*markers 17–23*, Fig. 1*B*), anterior leaflet edge markers (*markers 1–7*, Fig. 1*B*) and papillary tip markers (APM and PPM, Fig. 1*A*) were defined using actual marker data from IVR2 to IVR1.

The Hypermesh finite-element model (as in Fig. 4) was then solved for the enforced boundary conditions using Optistruct to obtain the simulated displacements of the leaflet belly markers (*markers 8–16*, Fig. 1*B*). This initial, nominal run assumed anterior MV leaflet material properties obtained from a previous ex vivo study (47).

Inverse finite-element analysis algorithm. The Optistruct solver was then interlinked with commercial optimization software (Hyperstudy version 8.0 SR 1, Altair Hyperworks) to run an inverse finite-element analysis (Fig. 5) to yield the in vivo material properties of the MV. In this algorithm, model-simulated displacements of the nine leaflet belly markers (*markers 8–16*, Fig. 1*B*) from the nominal run

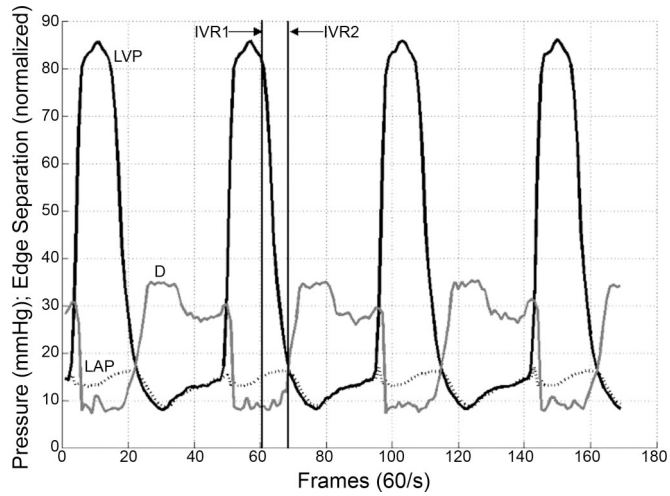

Fig. 3. Left ventricular pressure (LVP), LA pressure (LAP), and normalized distance between anterior and posterior leaflet edge markers (D, ×50) over 4 cardiac cycles from a representative heart. Isovolumic relaxation (IVR) was defined from the onset of IVR (IVR1) to the end of IVR (IVR2; reference state).

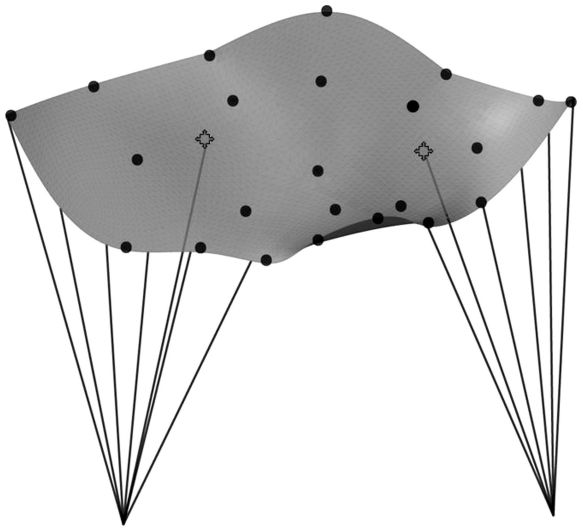

Fig. 4. Typical finite-element model developed by generating a bicubic surface (shown as translucent here) through the marker coordinates at IVR2 (●). Also shown are the primary and strut chordae modeled as tension-only PBARL elements radiating from the papillary muscle tips. Measured leaflet edge displacements were enforced, thus (although shown here) the primary chords were not required in the present study. Diamonds indicate the points of strut chord insertion.

were compared with actual measured displacements of these nine markers during IVR to yield an objective function defined as the root mean squared displacement difference between measured and actual displacements of the nine leaflet belly markers. Hyperstudy then used a parameter identification algorithm, the "method of feasible directions"(4), to minimize the objective function by repeated iterations of the material properties (E_{circ}, E_{rad}, and $G_{circ\text{-}rad}$) in the finite-element model until a global minimum was obtained (Fig. 6).

Using an absolute convergence value of 0.0001 cm (relative convergence of 0.01%) required 15 ± 3 iterations and 11 ± 2 min for each heartbeat analyzed. The material property values (E_{circ}, E_{rad}, and

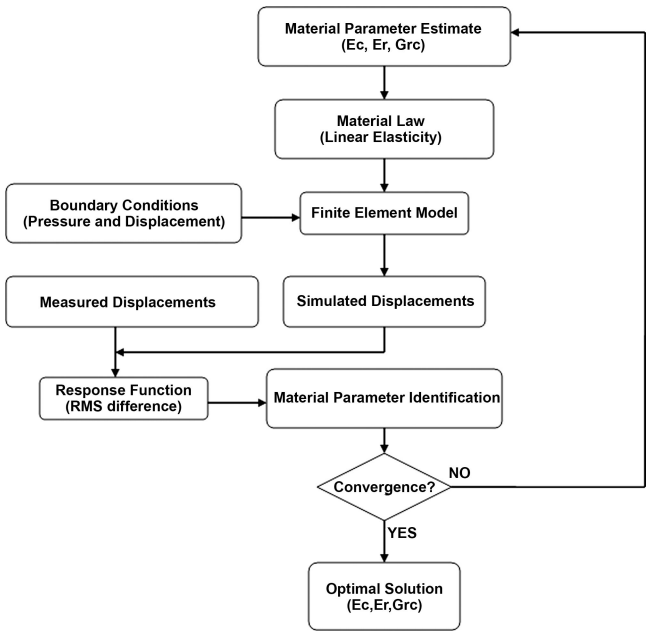

Fig. 5. Flow chart indicating the steps involved to solve for the in vivo anterior mitral valve leaflet material properties using the inverse finite-element analysis methodology. *E*, elastic modulus; *G*, shear modulus.

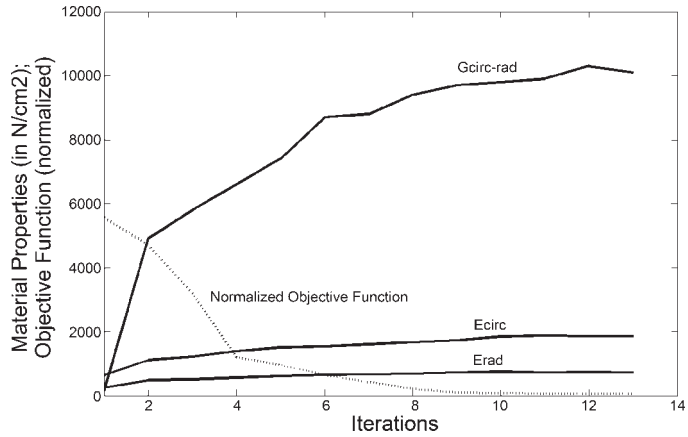

Fig. 6. Material properties [elastic modulus in the circumferential direction (E_{circ}), elastic modulus in the radial direction (E_{rad}), and leaflet shear modulus ($G_{circ\text{-}rad}$); all in N/cm^2] and normalized objective function (scaled automatically by Hyperstudy) versus the number of iterations in a representative experiment. The material properties were optimized using the method of feasible directions until a global minimum for the objective function was reached.

$G_{circ\text{-}rad}$) obtained at the end of the parameter identification run with the objective function at its global minimum were interpreted as the in vivo material properties of the anterior MV leaflet belly during IVR. That is, these material property values, when used in the finite-element model for the anterior leaflet belly under the enforced pressure and geometric boundary conditions, produced, as closely as possible, the same displacements of the nine leaflet belly markers as those measured experimentally during IVR. Figure 7*A* shows the measured displacements for a single heartbeat, and Fig. 7*B* shows the residuals between the measured and simulated displacements for all nine leaflet belly markers for a representative beat in one heart. The mean of all nine residuals for this one beat was 0.45 ± 0.20 mm. The convexity of the objective function was confirmed by seeding the optimization algorithm with very low and very high initial material property values. In both instances, the optimization process settled at the same unique minimum value of the objective function with the same parameter set. To further confirm the convexity of the objective function minimum, an experiment was performed wherein within a 30% range of the final material property values obtained from the optimization process, all combinations of E_{circ}, E_{rad}, and $G_{circ\text{-}rad}$ were systematically tested in steps of 1 N/mm^2, and a table of objective function values for different combinations of material property values was obtained. In this table, the global minimum of the objective function also corresponded to the same material property values obtained from the optimization process using the method of feasible directions; hence, this minimum appears to be unique.

Sensitivity Analysis

The sensitivity of inverse-finite element solutions to alterations in leaflet thickness and strut chord elastic modulus was examined. To study the change in leaflet material properties in response to leaflet thickness, the inverse-finite element analysis was performed on all beats with an increase in leaflet thickness to 2 mm at the annulus [approximating that reported at the annulus for normal human leaflets (22)], with a linear variation to 1.6 mm at the region 75% toward the leaflet free edge and thickness increased to 1.2 mm at the leaflet free edge to approximate the gradient observed in ovine leaflets. To examine the effect of a change in strut chord elastic modulus, inverse finite-element analyses were performed on all beats using chordal elastic moduli one-half (10 N/mm^2) or double (40 N/mm^2) the value obtained from previous ex vivo studies of porcine leaflets (32, 33).

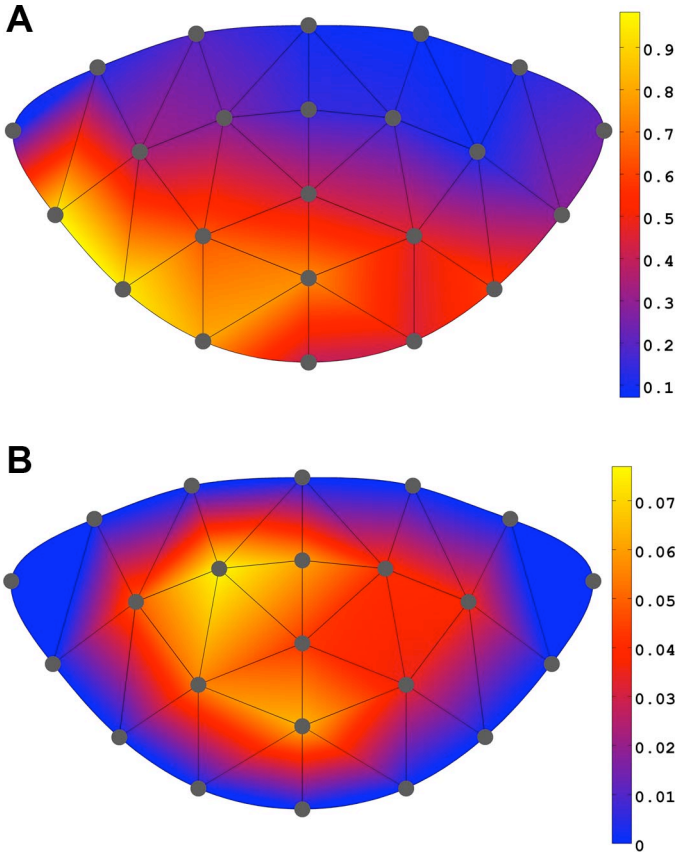

Fig. 7. *A*: schematic template as viewed from the LA showing color-coded measured displacements (laboratory coordinates, in cm) of the anterior mitral leaflet during IVR for 1 cardiac cycle in a representative heart. *B*: schematic template as viewed from the LA showing color-coded displacement residuals (in cm), the absolute value of the difference between actual measured anterior mitral valve leaflet displacements and the simulated displacements of the anterior mitral valve leaflet during IVR from the beat shown in *A*.

Statistical analysis. Fifty-one sets of material property values were obtained from this inverse finite-element analysis. Means and SDs for E_{circ}, E_{rad}, and $G_{circ\text{-}rad}$ were calculated for each set of 3 consecutive beats from each of the 17 hearts. A combined mean and SD for the entire study was also computed. A paired *t*-test (Sigmastat 2.03, SPSS, Chicago, IL) was performed between the overall average values of E_{circ} and E_{rad} to examine anisotropy of the anterior mitral leaflet. $P < 0.05$ was considered statistically significant. One-way ANOVA was performed to determine whether there was any intergroup variability for E_{circ}, E_{rad}, and $G_{circ\text{-}rad}$.

RESULTS

Hemodynamics

Table 1 shows the heart rate, $-dP/dt_{max}$ during IVR, and LVP and LAP at IVR1 and IVR2 used as boundary conditions in the finite-element model. These pressures varied little during sequential beats in each individual heart, but important variations were observed between hearts, providing a test of the robustness of the inverse finite-element approach under varied hemodynamic conditions.

Inverse Finite-Element Analysis Results

Table 2 shows $G_{circ\text{-}rad}$, E_{circ}, and E_{rad} of the anterior MV leaflet belly obtained from the inverse finite-element analysis algorithm for each beat in each heart. Residuals for each beat are also shown in Table 2. E_{circ} was significantly greater than E_{rad} for all hearts and all beats ($P < 0.01$), indicating that the anterior leaflet belly in vivo is significantly anisotropic, considerably stiffer in the circumferential than radial direction. There was no correlation between the material properties obtained and $-dP/dt_{max}$ during IVR (Tables 1 and 2), suggesting that viscosity does not play a significant role in these findings. These values also show that the in vivo material properties of the anterior leaflet belly are considerably higher than values previously reported from ex vivo studies (8, 10, 21, 22, 33, 42), suggesting that leaflets are much stiffer in the beating heart than when excised. E_{circ} in vivo was 5–12 times greater than posttransitional ex vivo values (21, 22, 33, 42), E_{rad} in vivo was 2–55 times stiffer than posttransitional ex vivo values (8, 10, 21, 22, 33, 42), and $G_{circ\text{-}rad}$ was 60–130 times greater than values assumed in a previous finite-element studu of the anterior leaflet (47). One-way ANOVA demonstrated intergroup variability for E_{circ} and $G_{circ\text{-}rad}$ but no significant intergroup variability for E_{rad}.

Sensitivity Analysis

Table 3 shows three-beat mean E_{circ}, E_{rad}, and $G_{circ\text{-}rad}$ values for each heart solved with leaflet thickness values much greater than those actually measured from sheep hearts, more nearly approximating those reported for normal human leaflets (22). Even with these abnormally large values of thickness, however, these ovine leaflet in vivo values were still considerably greater than those obtained from ex vivo studies, with E_{circ} being 1.9–3.0 times greater and E_{rad} 1.3–3.0 times greater than such ex vivo values (22).

Tables 4 and 5 show E_{circ}, E_{rad}, and $G_{circ\text{-}rad}$ values for each heart solved with strut chord stiffness twice and half, respectively, of the ex vivo strut chordae value (20 N/mm^2) used in the present study (33). A large increase or decrease in the elastic modulus of these strut chords had only a very minor effect on the resultant material properties for the anterior MV leaflet belly computed using this inverse finite-element approach. Note that the strut chordae material properties only constrain the displacement of those second-order chords that attach to the leaflet belly. Because the motion of the leaflet edge is constrained in the model to move as it does experimentally, the material properties of the primary chordae, as well as any effect of the posterior leaflet pressing against the anterior leaflet, have no effect on these results.

The centroid of each marker in each time frame of the two-dimensional images was digitized by experienced personnel using custom software. Tests of interdigitizer variability in the selection of marker centroids with three independent digitizers produced <2% variability in E_{circ}, <1% variability in E_{rad}, and <4% variability in $G_{circ\text{-}rad}$. Thus, small variations in the *x*-, *y*-, and z-coordinates of the markers selected by different digitizers did not significantly alter the material properties reported here.

DISCUSSION

The principal finding of this study is that ovine anterior MV leaflets in vivo are considerably stiffer than values reported for excised porcine or human anterior leaflets. Previous ex vivo studies (8, 22, 33, 42) have found posttransitional leaflet E_{rad}

Table 1. *Hemodynamics*

Experiment	Heart Rate, beats/min	LV $-dP/dt_{max}$ During IVR, mmHg/s	LVP at IVR1, mmHg	LVP at IVR2, mmHg	LAP at IVR1, mmHg	LAP at IVR2, mmHg
1	77	1,592±46	82 ± 1	11 ± 0	10 ± 0	7 ± 1
2	89	1,560±109	92±1	11±1	8±0	8±0
3	95	905±27	61±2	11±1	5±0	5±0
4	97	1,787±55	99±4	12±1	8±0	7±0
5	107	1,967±123	67±1	10±1	2±0	2±1
6	99	1,120±24	91±1	18±0	1±0	1±0
7	93	1,003±11	95±1	11±2	13±0	9±1
8	93	1,103±39	88±1	12±0	14±0	9±0
9	95	1,284±53	87±1	14±1	11±0	12±0
10	80	858±21	83±0	11±0	11±0	11±0
11	70	991±19	84±1	6±1	8±1	4±1
12	97	1,425±29	85±0	10±1	9±0	9±0
13	70	1,158±15	90±0	9±0	10±0	9±0
14	78	1,439±29	90±0	6±0	7±0	6±0
15	107	1,721±77	98±0	7±0	6±0	6±1
16	80	1,621±69	84±2	4±1	5±1	4±1
17	82	1,346±327	95±4	7±1	8±0	7±0
Group mean ± SD	89±11	1,345±320	87±10	10±3	8±3	7±3

Shown are heart rate, left ventricular (LV) $-dP/dt_{max}$ during isovolumic relaxation (IVR), and LV pressure (LVP) and left atrial pressure (LAP) at the onset of IVR (IVR1) and end of IVR (IVR2) for three sequential beats analyzed from each heart. LVP at IVR1, LVP at IVR2, LAP at IVR1, and LAP at IVR2 were used as boundary conditions in the finite-element model.

values ranging from 0.2 to 5 N/mm^2, whereas E_{rad} values in the present in vivo study ranged from 4 to 18 N/mm^2. These previous ex vivo studies found posttransitional E_{circ} values ranging from 3.6 to 9 N/mm^2, whereas E_{circ} values in the present in vivo study ranged from 13–97 N/mm^2. It should be noted, however, that it is not clear that leaflet strains in vivo place the leaflet in the posttransitional region of the ex vivo stress-strain relationship. If, in fact, they operate in the pretransitional region, which seems quite likely, then the stiffness disparity between in vivo and ex vivo results is even greater, by one to two orders of magnitude.

Another finding from the present study is that the ovine leaflet belly in vivo exhibits the same significant leaflet anisotropy previously observed in leaflet ex vivo studies, with E_{circ} considerably greater than E_{rad}. In keeping with this finding, previous ex vivo studies have shown that anterior leaflets exhibit large radial (4–30%) and smaller circumferential (2–11%) maximal stretch under full loading conditions (6, 7, 25, 29, 49).

The large anterior leaflet stiffness found in this study has at least two plausible explanations. The first and most obvious possibility is that the thinner ovine leaflets are actually considerably stiffer than human and porcine leaflets, which themselves have quite similar material properties (22, 42). This possibility needs to be addressed by future biaxial studies of excised ovine anterior leaflets.

A second possibility, as discussed by Williams and Jew (59), is that leaflets in vivo are active structures, and this activity is lost when leaflets are excised for static testing. There are several indirect lines of evidence supporting this hypothesis.

Table 2. *Material properties of the anterior leaflet belly*

Experiment	E_{circ}, N/mm^2	E_{rad}, N/mm^2	$G_{circ\text{-}rad}$, N/mm^2	Mean of Residuals, mm
1	18, 16, 13	7, 9, 9	101, 118, 149	0.47
2	31, 22, 37	9, 4, 8	180, 190, 175	0.23
3	82, 97, 65	13, 9, 11	161, 117, 132	0.43
4	79, 65, 74	14, 8, 11	79, 97, 101	0.36
5	22, 19, 32	8, 14, 7	110, 179, 142	0.27
6	43, 56, 52	18, 12, 17	128, 137, 112	0.69
7	36, 43, 56	8, 9, 14	97, 108, 86	0.28
8	19, 16, 23	7, 7, 9	88, 97, 89	0.55
9	16, 22, 18	6, 9, 11	102, 107, 124	0.39
10	44, 39, 37	11, 11, 14	110, 121, 115	0.31
11	62, 71, 55	12, 18, 11	118, 132, 116	0.71
12	49, 42, 38	16, 14, 18	111, 117, 104	0.65
13	33, 29, 39	19, 11, 13	143, 136, 144	0.22
14	57, 51, 51	9, 7, 9	98, 94, 101	0.19
15	24, 28, 29	9, 12, 10	143, 127, 129	0.28
16	67, 59, 57	14, 14, 18	111, 129, 113	0.22
17	46, 49, 41	9, 8, 13	121, 137, 134	0.43
Group mean ± SD (n = 17)	43±18*	11±3	121±22	0.39±0.17

Shown are the elastic modulus in the circumferential direction (E_{circ}), elastic modulus in the radial direction (E_{rad}), and leaflet shear modulus ($G_{circ\text{-}rad}$) for three heart beats (values for each heart beat separated by commas) in each animal from the inverse finite-element analysis. The mean of the nine leaflet belly marker residuals is also shown for each experiment. *$P < 0.01$, E_{circ} vs. E_{rad}.

Table 3. *Sensitivity test of thicker valves*

Experiment	E_{circ}, N/mm^2	E_{rad}, N/mm^2	$G_{circ\text{-}rad}$, N/mm^2	Mean of Residuals, mm
1	7±0	3±1	8±1	0.38
2	9±2	5±2	7±3	0.41
3	7±1	3±1	11±1	0.33
4	11±2	7±2	11±4	0.63
5	10±1	5±0	7±0	0.45
6	8±1	4±1	13±1	0.29
7	7±3	3±1	11±4	0.40
8	10±1	6±2	15±3	0.71
9	14±3	6±1	12±2	0.43
10	7±4	4±2	11±3	0.38
11	11±1	4±3	15±3	0.33
12	13±2	5±2	12±2	0.29
13	8±1	5±3	11±3	0.21
14	10±2	4±2	13±3	0.39
15	10±1	5±1	14±3	0.47
16	6±3	2±1	9±2	0.60
17	9±1	7±2	11±2	0.55
Group mean ± SD	9±2	5±1	11±2	0.42±0.13

Values are means ± SD of material properties determined using anterior mitral valve leaflet thickness values approximating those reported for normal human leaflets (22). The inverse finite-element analysis was performed on all animals for three heart beats each by increasing the leaflet thickness to 2 mm at the annulus, varying linearly to 1.6 mm at the region 75% toward the leaflet free edge. Thickness was increased to 1.2 mm at the leaflet free edge. The mean of nine leaflet belly marker residuals is also shown for each experiment.

Complex Anterior Leaflet Constituents

For a recent review of complex anterior leaflet constituents, see Ref. 50. In addition to complex collagen networks (8, 11, 18, 19, 24, 37) and lymphatic and blood vessels (12, 19), anterior MV leaflets contain a number of constituents capable of actively modifying leaflet stiffness, such as various types of muscle fibers (5, 12, 16–19, 26, 45, 54, 55, 61, 62) and interstitial cells (9, 20, 23, 37, 53). Ablation of annular and leaflet musculature on the atrial side of the valve alters the shape of the anterior leaflet during and after closure (55).

Table 4. *Sensitivity test of increased chordal stiffness*

Experiment	E_{circ}, N/mm^2	E_{rad}, N/mm^2	$G_{circ\text{-}rad}$, N/mm^2	Mean of Residuals, mm
1	16±2	8±1	111±10	0.37
2	29±6	7±2	173±9	0.48
3	80±13	10±2	132±20	0.63
4	72±6	10±2	91±10	0.33
5	22±5	8±3	140±24	0.19
6	44±4	14±3	121±10	0.27
7	42±6	9±2	92±5	0.23
8	18±3	8±1	88±5	0.65
9	19±2	7±3	106±8	0.27
10	36±4	11±2	108±4	0.39
11	60±7	11±4	118±5	0.31
12	41±3	15±2	106±7	0.27
13	32±4	13±2	137±11	0.21
14	52±3	7±1	96±4	0.46
15	24±4	8±2	129±6	0.66
16	58±3	14±2	114±13	0.39
17	42±5	8±3	128±9	0.34
Group mean ± SD	40±18	10±3	117±21	0.38±0.15

Values are means ± SD of material properties for each heart with chordal elastic moduli twice (40 N/mm^2) those obtained from a previous study of excised chordae tendinae (33). The mean of the nine leaflet belly marker residuals is also shown for each experiment.

Table 5. *Sensitivity test of decreased chordal stiffness*

Experiment	E_{circ}, N/mm^2	E_{rad}, N/mm^2	$G_{circ\text{-}rad}$, N/mm^2	Mean of Residuals, mm
1	19±2	11±2	147±12	0.51
2	34±6	9±2	185±4	0.46
3	84±13	14±2	153±18	0.39
4	76±5	14±2	99±10	0.35
5	25±7	11±3	158±31	0.29
6	53±6	17±3	130±10	0.21
7	47±7	12±2	105±8	0.20
8	22±2	9±1	94±4	0.36
9	21±3	11±1	114±10	0.28
10	45±5	13±2	119±7	0.44
11	64±4	17±4	129±13	0.39
12	45±6	17±3	112±6	0.33
13	34±4	16±3	145±7	0.50
14	55±4	9±2	103±5	0.41
15	30±3	12±2	139±6	0.49
16	62±3	16±3	120±8	0.52
17	49±5	11±1	135±10	0.44
Group mean ± SD	45±19	13±3	129±23	0.38±0.10

Values are means ± SD of material properties for each heart with chordal elastic moduli half (10 N/mm^2) those obtained from a previous study of excised chordae tendinae (33). The mean of the nine leaflet belly marker residuals is also shown for each experiment.

Electrical Activity

Leaflets are electrically active (18, 45, 60–62), with electrical coupling to the LA (13, 62). Electrical stimulation occurs during each heart beat, which could trigger alterations in leaflet material properties.

Neuromuscular Control

Leaflets contain a profusion of both afferent and efferent motor and sensory nerves (1, 2, 12, 15, 16, 19, 26, 28, 31, 40, 44, 52, 56–58) and are possibly under neuromuscular control (54). They are capable of responding to sympathetic and parasympathetic stimulation and changing their stiffness during the cardiac cycle, provided that leaflet muscle is undamaged (13). It has been hypothesized that the vagus nerve endings in the valve affect myocyte contraction in the valve and change the structural tone of the valve in response to stress (31).

Differentiating between these possibilities is an ongoing subject of research in these laboratories.

In addition to helping improve our understanding of MV physiology in vivo, further refinement of this finite-element approach, with material parameters derived from experimental data, could potentially improve the design of bioprostheses as well as aid in the development of durable tissue-engineered bioprosthetic valves. Sufficiently refined, such a model might also be employed to assist the planning of patient-specific operations with targeted objectives in the computer before these procedures are carried out in the operating room.

Limitations

This inverse finite-element methodology appears to be a robust initial approach to quantify the elastic and rigidity moduli of the anterior MV leaflet belly in the beating heart. The present study, however, represents only a first attempt to derive these values in vivo and has a number of current

limitations that must be addressed in more sophisticated future studies.

Leaflet thickness. In the present study, leaflet thickness value distributions applied in the finite-element model were obtained from a detailed examination of a representative ovine anterior leaflet. Since leaflet deformation is predominantly determined by bending and the bending stiffness is proportional to the thickness cubed, it is not surprising that the parameter identification is very sensitive to thickness changes. Ultimately, regional thickness values for each heart need to be applied to the model, and this work is underway. A previous ex vivo study (22) of thicker human leaflets found lower elastic moduli than those obtained from the present study. However, even when these greater thickness values were applied to the ovine model, in vivo ovine elastic moduli were still greater than those reported from ex vivo studies (Table 3).

Homogeneous leaflet material properties. Leaflets are known to be heterogeneous, with different regions of the leaflet having different material properties (8). Scanning acoustic microscopy has indicated that human anterior leaflets are stiffer in the fibrous middle layer than atrial and ventricular layers and the entire leaflet is stiffer at the annulus than at the free edge (27). Leaflet homogeneity was a simplification for this initial effort to quantify the in vivo material properties of the belly of the anterior MV leaflet. Figure 7*B* shows heterogenous residuals suggesting material property heterogeneity, but most residuals were between 0.2 and 0.7 mm; thus, the leaflet belly may not exhibit significant regional heterogeneity. Nevertheless, heterogeneity is an important issue that will be addressed in future studies.

Assumption of three-parameter linear elasticity. The initial strain estimates from preliminary, direct calculations of regional MV leaflet strain have indicated that the strains during IVR in the ovine leaflet belly are <0.15. May-Newman and Yin (42) found that the stress-strain curves of the porcine anterior leaflet ex vivo are quite linear for strains $<15\%$. Thus, a linear stress-strain assumption may be provisionally valid during IVR, and a single linear elastic modulus is reported here. The present study, however, was not designed to assess the shape of the stress-strain relation in the ovine leaflet in vivo, and this is the subject of future work. Studies of the material properties of excised leaflets (22, 33, 42) have clearly demonstrated a pretransitional/posttransitional breakpoint in the stress-strain curve, and this is usually attributed to the behavior of coiled/uncoiled collagen fibers. However, Sonnenblick et al. (54) found a simple exponential stress-strain relationship, with no apparent breakpoint, in fresh canine anterior leaflet tissue placed in a myograph containing oxygenated Krebs solution at 30°C and capable of developing active tension in response to electrical stimulation. This raises the possibility that treating the leaflet tissue as an active contractile system (54) converts ex vivo experiments from a study of collagen fibers to a study of collagen fibers plus active contractile tissue having an entirely different stress-strain relationship. Furthermore, even the tissue studied by Sonnenblick et al. (54) lacked blood perfusion and the neural inputs present in vivo. Thus, it is quite possible that leaflets do not behave as simple collagen networks in the beating heart but rather as active contractile tissue with stress-strain behavior unlike that observed in any ex vivo test.

Limited number of leaflet markers. More markers would always be advantageous to better define leaflet geometry, but 16 radiopaque leaflet markers (*markers 1–16*, Fig. 1*B*) are the most that can currently be placed, taking into consideration the size of the leaflet, cardiopulmonary bypass time, and X-ray reconstruction issues. The mass of each leaflet marker is ~3.2 mg. If the markers were very massive, then the measured deformations could include momentum effects in addition to pressure-induced displacements, although this would be expected to be very small as leaflet velocities during IVR are almost negligible. In a previous study (36), we demonstrated that an anterior leaflet marker mass 3.5 times greater than the marker mass in the present study had no effect on the peak opening velocity of the anterior leaflet relative to leaflets with no markers implanted (0.47 ± 0.05 vs. 0.45 ± 0.06 m/s). Thus, even with grossly overloaded leaflets and the high opening velocities associated with valve opening, we were unable to detect an effect of marker mass on leaflet mechanics, much less during the extremely low velocities of the closed valve during IVR, as is the case in the present study.

Incorrectly placed strut chordae. The strut chordae in the finite-element model were placed according to anatomic locations using photographs of excised anterior leaflets from each heart studied. Strut chordal insertion into the leaflet belly, however, is more complex than simple points of attachment, and this must be the direction of future work to improve the anatomic reconstruction of the model.

GRANTS

This work was supported by National Heart, Lung, and Blood Institute (NHLBI) Grants HL-29589 and HL-67025. W. Bothe was supported by the Deutsche Herzstiftung (Frankfurt, Germany). D. B. Ennis was supported by NHLBI Pathway to Independence Grant K99-R00-HL-087614.

REFERENCES

1. **Ahmed A, Johansson O, Folan-Curran J.** Distribution of PGP 95, TH, NPY, SP and CGRP immunoreactive nerves in the rat and guinea pig atrioventricular valves and chordae tendineae. *J Anat* 191: 547–560, 1997.
2. **Anderson RH.** The disposition and innervation of atrioventricular ring specialized tissue in rats and rabbits. *J Anat* 113: 197–211, 1972.
3. **Antunes MJ.** *Mitral Valve Repair*. Percha, Germany: Schulz, 1989.
4. **Belegundu AD, Damle A, Rajan SD, Dattaguru B, St. Ville J.** Parallel line search in method of feasible directions. *Optim Eng* 5: 379–388, 2004.
5. **Boucek RJ, Bouckova B, Levy S.** Anatomical arrangement of muscle tissue in the anterior mitral leaflet in man. *Cardiovasc Res* 12: 675–680, 1978.
6. **Chen L, May-Newman K.** Effect of strut chordae transection on mitral valve leaflet biomechanics. *Ann Biomed Eng* 34: 917–926, 2006.
7. **Chen L, McCulloch AD, May-Newman K.** Nonhomogeneous deformation in the anterior leaflet of the mitral valve. *Ann Biomed Eng* 32: 1599–1606, 2004.
8. **Chen L, Yin FC, May-Newman K.** The structure and mechanical properties of the mitral valve leaflet-strut chordae transition zone. *J Biomech Eng* 126: 244–251, 2004.
9. **Chester AH, Taylor PM.** Molecular and functional characteristics of heart-valve interstitial cells. *Philos Trans R Soc Lond B Biol Sci* 362: 1437–1443, 2007.
10. **Clark RE.** Stress-strain characteristics of fresh and frozen human aortic and mitral leaflets and chordae tendineae. Implications for clinical use. *J Thorac Cardiovasc Surg* 66: 202–208, 1973.
11. **Cochran RP, Kunzelman KS, Chuong CJ, Sacks MS, Eberhart RC.** Nondestructive analysis of mitral valve collagen fiber orientation. *ASAIO Trans* 37: M447–448, 1991.
12. **Cooper T, Napolitano L, Fitzgerald M, Moore K, Daggett W, Willman V, Sonnenblick E, Hanlon C.** Structural basis for cardiac valvular function. *Arch Surg* 93: 767–771, 1966.
13. **Curtis MB, Priola DV.** Mechanical properties of the canine mitral valve: effects of autonomic stimulation. *Am J Physiol Heart Circ Physiol* 262: H56–H62, 1992.
14. **Daughters GT, Sanders WJ, Miller DC, Schwarzkopf A, Mead CW, Ingels NBJ.** A comparison of two analytical systems for 3-D reconstruction from biplane videoradiograms. *IEEE Comp Cardiol* 15: 79–82, 1989.

15. **De Biasi S, Vitellaro-Zuccarello L, Blum I.** Histochemical and ultrastructural study on the innervation of human and porcine atrio-ventricular valves. *Anat Embryol (Berl)* 169: 159–165, 1984.
16. **Ellison JP, Hibbs RG.** The atrioventricular valves of the guinea-pig. I. A light microscopic study. *Am J Anat* 138: 331–345, 1973.
17. **Erlanger J.** A note on the contractility of the musculature of the auriculo-ventricular valves. *Am J Physiol* 40: 150–151, 1916.
18. **Fenoglio J Jr, Tuan DP, Wit AL, Bassett AL, Wagner BM.** Canine mitral complex Ultrastructure and electromechanical properties. *Circ Res* 31: 417–430, 1972.
19. **Filip DA.** Mouse atrio-ventricular valve ultrastructure morphometrical correlations. *Morphol Embryol (Bucur)* 30: 165–173, 1984.
20. **Filip DA, Radu A, Simionescu M.** Interstitial cells of the heart valves possess characteristics similar to smooth muscle cells. *Circ Res* 59: 310–320, 1986.
21. **Ghista DN, Rao AP.** Structural mechanics of the mitral valve: stresses sustained by the valve; non-traumatic determination of the stiffness of the in vivo valve. *J Biomech* 5: 295–307, 1972.
22. **Grande-Allen KJ, Barber JE, Klatka KM, Houghtaling PL, Vesely I, Moravec CS, McCarthy PM.** Mitral valve stiffening in end-stage heart failure: evidence of an organic contribution to functional mitral regurgitation. *J Thorac Cardiovasc Surg* 130: 783–790, 2005.
23. **Grande-Allen KJ, Calabro A, Gupta V, Wight TN, Hascall VC, Vesely I.** Glycosaminoglycans and proteoglycans in normal mitral valve leaflets and chordae: association with regions of tensile and compressive loading. *Glycobiology* 14: 621–633, 2004.
24. **Hadian M, Corcoran BM, Han RI, Grossmann JG, Bradshaw JP.** Collagen organization in canine myxomatous mitral valve disease: an x-ray diffraction study. *Biophys J* 93: 2472–2476, 2007.
25. **He Z, Sacks MS, Baijens L, Wanant S, Shah P, Yoganathan AP.** Effects of papillary muscle position on in-vitro dynamic strain on the porcine mitral valve. *J Heart Valve Dis* 12: 488–494, 2003.
26. **Hibbs RG, Ellison JP.** The atrioventricular valves of the guinea-pig. II. An ultrastructural study. *Am J Anat* 138: 347–369, 1973.
27. **Jensen AS, Baandrup U, Hasenkam JM, Kundu T, Jorgensen CS.** Distribution of the microelastic properties within the human anterior mitral leaflet. *Ultrasound Med Biol* 32: 1943–1948, 2006.
28. **Jew JY, Fink CA, Williams TH.** Tyrosine hydroxylase- and nitric oxide synthase-immunoreactive nerve fibers in mitral valve of young adult and aged Fischer 344 rats. *J Auton Nerv Syst* 58: 35–43, 1996.
29. **Jimenez JH, Liou SW, Padala M, He Z, Sacks M, Gorman RC, Gorman JH 3rd, Yoganathan AP.** A saddle-shaped annulus reduces systolic strain on the central region of the mitral valve anterior leaflet. *J Thorac Cardiovasc Surg* 134: 1562–1568, 2007.
30. **Karlsson MO, Glasson JR, Bolger AF, Daughters GT, Komeda M, Foppiano LE, Miller DC, Ingels NB Jr.** Mitral valve opening in the ovine heart. *Am J Physiol Heart Circ Physiol* 274: H552–H563, 1998.
31. **Kawano H, Kawai S, Shirai T, Okada R.** Morphological study on vagal innervation in human atrioventricular valves using histochemical method. *Jpn Circ J* 57: 753–759, 1993.
32. **Kunzelman KS, Cochran RP.** Mechanical properties of basal and marginal mitral valve chordae tendineae. *ASAIO Trans* 36: M405–M408, 1990.
33. **Kunzelman KS, Cochran RP.** Stress/strain characteristics of porcine mitral valve tissue: parallel versus perpendicular collagen orientation. *J Card Surg* 7: 71–78, 1992.
34. **Kunzelman KS, Cochran RP, Chuong C, Ring WS, Verrier ED, Eberhart RD.** Finite element analysis of the mitral valve. *J Heart Valve Dis* 2: 326–340, 1993.
35. **Kunzelman KS, Einstein DR, Cochran RP.** Fluid-structure interaction models of the mitral valve: function in normal and pathological states. *Philos Trans R Soc Lond B Biol Sci* 362: 1393–1406, 2007.
36. **Langer F, Tibayan FA, Rodriguez F, Timek T, Zasio MK, Liang D, Daughters GT, Ingels NB, Miller DC.** Altered mitral valve kinematics with atrioventricular and ventricular pacing. *J Heart Valve Dis* 14: 286–294, 2005.
37. **Latif N, Sarathchandra P, Taylor PM, Antoniw J, Yacoub MH.** Localization and pattern of expression of extracellular matrix components in human heart valves. *J Heart Valve Dis* 14: 218–227, 2005.
38. **Levine RA, Handschumacher MD, Sanfilippo AJ, Hagege AA, Harrigan P, Marshall JE, Weyman AE.** Three-dimensional echocardiographic reconstruction of the mitral valve, with implications for the diagnosis of mitral valve prolapse. *Circulation* 80: 589–598, 1989.
39. **Lim KH, Yeo JH, Duran CM.** Three-dimensional asymmetrical modeling of the mitral valve: a finite element study with dynamic boundaries. *J Heart Valve Dis* 14: 386–392, 2005.
40. **Lipp W, Rodin M.** The adrenergic nerve plexuses of cardiac valves. *Acta Anat (Basel)* 69: 313–326, 1968.
41. **Maisano F, Redaelli A, Soncini M, Votta E, Arcobasso L, Alfieri O.** An annular prosthesis for the treatment of functional mitral regurgitation: finite element model analysis of a dog bone-shaped ring prosthesis. *Ann Thorac Surg* 79: 1268–1275, 2005.
42. **May-Newman K, Yin FC.** Biaxial mechanical behavior of excised porcine mitral valve leaflets. *Am J Physiol Heart Circ Physiol* 269: H1319–H1327, 1995.
43. **Niczyporuk MA, Miller DC.** Automatic tracking and digitization of multiple radiopaque myocardial markers. *Comput Biomed Res* 24: 129–142, 1991.
44. **Oki T, Fukuda N, Kawano T, Iuchi A, Tabata T, Manabe K, Kageji Y, Sasaki M, Yamada H, Ito S.** Histopathologic studies of innervation of normal and prolapsed human mitral valves. *J Heart Valve Dis* 4: 496–502, 1995.
45. **Priola DV, Fulton RL, Napolitano LM, Cooper T.** Electrical activity of the canine mitral valve in situ. *Am J Physiol* 216: 238–243, 1969.
46. **Prot V, Haaverstad R, Skallerud B.** Finite element analysis of the mitral apparatus: annulus shape effect and chordal force distribution. *Biomech Model Mechanobiol*. In press.
47. **Reimink MS, Kunzelman KS, Cochran RP.** The effect of chordal replacement suture length on function and stresses in repaired mitral valves: a finite element study. *J Heart Valve Dis* 5: 365–375, 1996.
48. **Rodriguez F, Langer F, Harrington KB, Tibayan FA, Zasio MK, Liang D, Daughters GT, Ingels NB, Miller DC.** Effect of cutting second-order chordae on in-vivo anterior mitral leaflet compound curvature. *J Heart Valve Dis* 14: 592–601, 2005.
49. **Sacks MS, Enomoto Y, Graybill JR, Merryman WD, Zeeshan A, Yoganathan AP, Levy RJ, Gorman RC, Gorman JH 3rd.** In-vivo dynamic deformation of the mitral valve anterior leaflet. *Ann Thorac Surg* 82: 1369–1377, 2006.
50. **Sacks MS, Yoganathan AP.** Heart valve function: a biomechanical perspective. *Philos Trans R Soc Lond B Biol Sci* 362: 1369–1391, 2007.
51. **Salgo IS, Gorman JH, Gorman RC 3rd, Jackson BM, Bowen FW, Plappert T, St. John Sutton MG, Edmunds LH Jr.** Effect of annular shape on leaflet curvature in reducing mitral leaflet stress. *Circulation* 106: 711–717, 2002.
52. **Smith RB.** Intrinsic innervation of the atrioventricular and semilunar valves in various mammals. *J Anat* 108: 115–121, 1971.
53. **Smith S, Taylor PM, Chester AH, Allen SP, Dreger SA, Eastwood M, Yacoub MH.** Force generation of different human cardiac valve interstitial cells: relevance to individual valve function and tissue engineering. *J Heart Valve Dis* 16: 440–446, 2007.
54. **Sonnenblick EH, Napolitano LM, Daggett WM, Cooper T.** An intrinsic neuromuscular basis for mitral valve motion in the dog. *Circ Res* 21: 9–15, 1967.
55. **Timek TA, Lai DT, Dagum P, Tibayan F, Daughters GT, Liang D, Berry GJ, Miller DC, Ingels NB Jr.** Ablation of mitral annular and leaflet muscle: effects on annular and leaflet dynamics. *Am J Physiol Heart Circ Physiol* 285: H1668–H1674, 2003.
56. **Williams TH.** Fast-conducting fibres in the mitral valve. *Br Heart J* 26: 554–557, 1964.
57. **Williams TH.** Mitral and tricuspid valve innervation. *Br Heart J* 26: 105–115, 1964.
58. **Williams TH, Folan JC, Jew JY, Wang YF.** Variations in atrioventricular valve innervation in four species of mammals. *Am J Anat* 187: 193–200, 1990.
59. **Williams TH, Jew JY.** Is the mitral valve passive flap theory overstated? An active valve is hypothesized. *Med Hypotheses* 62: 605–611, 2004.
60. **Wit AL, Cranefield PF.** Triggered activity in cardiac muscle fibers of the simian mitral valve. *Circ Res* 38: 85–98, 1976.
61. **Wit AL, Fenoglio J Jr, Hordof AJ, Reemtsma K.** Ultrastructure and transmembrane potentials of cardiac muscle in the human anterior mitral valve leaflet. *Circulation* 59: 1284–1292, 1979.
62. **Wit AL, Fenoglio J Jr, Wagner BM, Bassett AL.** Electrophysiological properties of cardiac muscle in the anterior mitral valve leaflet and the adjacent atrium in the dog. Possible implications for the genesis of atrial dysrhythmias. *Circ Res* 32: 731–745, 1973.